ADVANCED MATERIALS

[24] M. Scholl, S. Ding, C. W. Lee, R. H. Grubbs, *Org. Lett.* **1999**, *1*, 953.
[25] M. S. Sanford, J. A. Love, R. H. Grubbs, *Organometallics* **2001**, *20*, 5314.
[26] J. A. Love, J. P. Morgan, T. M. Trnka, R. H. Grubbs, *Angew. Chem. Int. Ed.* **2002**, *41*, 4035.
[27] R. H. Grubbs, C. S. Woodson, Jr., *US Patent 9 703 096*, **1997**.
[28] R. F. Cunico, *J. Org. Chem.* **1971**, *36*, 929.

Three-Dimensionally Oriented Aggregation of a Few Hundred Nanoparticles into Monocrystalline Architectures**

By *Zhongping Zhang*, *Haiping Sun*, *Xiaoqiong Shao*, *Dongfei Li*, *Haidong Yu*, and *Mingyong Han**

Surface-stabilized nanoparticles, acting as nanoscale building blocks, can spontaneously self-assemble into various ordered nanostructures, a process which is usually controlled by altering the surface properties of particles using organic-coating layers.[1–5] It has been well established that organic ligands with high nanoparticle binding affinities can promote self-assembly, driven by the interactions between surface-adsorbed ligands instead of between the particles themselves. In the absence of sufficiently strong surface-protecting layers, it seemed that nanoparticles would always randomly aggregate into disordered solids. However, recent demonstrations of self-organized aggregation of such nanoparticles to yield ordered-crystal structures came as a surprise.[6–10] Ordered self-assembly requires that aggregated nanoparticles can equilibrate with non-aggregated ones in solution and adjust their positions relative to one another in an aggregate. The aggregation-driven growth of nanoparticles into single-crystalline architectures is usually realized upon the controlled removal of appropriate organic additives at interfaces and the subsequent oriented attachment of nanoparticles by rotating adjacent nanoparticles so that they share an identical crystallographic orientation.[8,11] The normal concept for crystal growth, which is typically thought to occur via atom-by-atom addition to an existing nucleus or template, has been challenged by the aggregation-based growth of nanoparticles. A few examples of aggregation-based growth have been reported recently, such as the fusion growth of Ag nanoparticles into nanoprisms,[12] the ligand-directed assembly of preformed titania nanocrystals into highly anisotropic nanostructures,[13] and the spontaneous aggregation of iron oxyhydroxide into larger defective monocrystals in iron-oxidizing bacteria.[6] In addition, oriented aggregation of nanoparticles has also led to the formation of other low-dimensional crystalline materials such as ZnO nanorods,[7] CdTe nanowires,[8] and α-Fe_2O_3 disks/ellipsoids.[14,15]

Since the oriented-aggregation growth of a limited number of nanoparticles into low-dimensional crystalline nanomaterials has been demonstrated through linearly oriented attachment, it is our goal to observe and understand the three-dimensional (3D) orientation and aggregation process of a few hundred nanoparticles into a single-crystalline 3D structure. Here we report a simple synthetic approach to building monocrystalline CuO from nanoparticles at room temperature. We have demonstrated an anisotropic aggregation-based crystal-growth process of a few hundred monoclinic CuO nanoparticles into uniform ellipsoidal monocrystalline architectures. Stepwise orientation and aggregation of a large number of nanoparticles in three dimensions has been observed, from the formation of primary CuO nanoparticles, to the preferential one-dimensional (1D) orientation of nanoparticles along the (001) direction at an early stage, and, eventually, 3D-oriented aggregation into a monocrystalline structure built from nanoparticles. Selective adsorption of formamide molecules on different crystallographic planes of monoclinic CuO nanoparticles may play an important role in the anisotropic growth of uniform nanoparticle-built monocrystals. The understanding of the oriented-attachment mechanism may further open up new opportunities to fabricate complex low-dimensional or 3D nanostructured materials and provide new insight into the aggregated biomineralization mechanism of nanoparticles.

Copper oxide has been of considerable interest because it forms the basis of technologically important materials such as high-temperature superconductors and plays practical roles in catalysis, sensing, and solar-energy transformation.[16–20] The ability to fabricate nanostructured copper oxide has further prompted a renewed interest in enriching our understanding of its fundamental properties and enhancing its performance in currently existing applications. Copper oxide nanoparticles have recently been prepared by a number of methods, including thermal decomposition, oxidation, reduction, and hydrolysis of metal or metal salts.[16–21] In the research reported here, aggregation-based formation of nanostructured copper oxide particles has been achieved through a simple natural oxidation of copper metal in formamide and subsequent hydrolysis of the resulting copper–formamide complexes in aqueous solution, as detailed in the Experimental section. The powder X-ray diffraction (XRD) pattern of the as-synthesized sample in Figure 1A confirms the formation of crystalline monoclinic CuO (cupric oxide) (Joint Committee on Powder Diffraction Standards file No. 74-1021). Uniform ellipsoidal particles of cupric oxide were revealed by low-magnification transmission

[*] Prof. M. Han, Dr. Z. Zhang, Dr. H. Sun, Dr. D. Li
Institute of Materials Research and Engineering
3 Research Link, Singapore 117602 (Singapore)
E-mail: my-han@imre.a-star.edu.sg
Prof. M. Han, X. Shao, H. Yu
Department of Materials Science
National University of Singapore
Singapore 119260 (Singapore)

[**] This work was supported by the Institute of Materials Research & Engineering and the National University of Singapore.

  DOI: 10.1002/adma.200400401

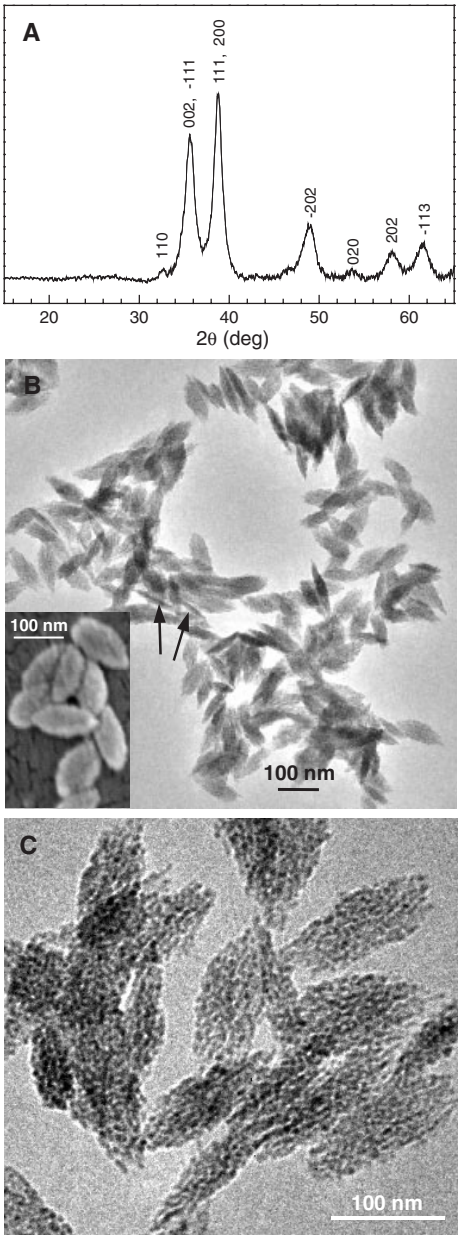

Figure 1. A) Powder XRD pattern and B,C) transmission electron microscopy (TEM) images of the as-synthesized nanoarchitectures of cupric oxide. (B) is an overview TEM image (inset: corresponding scanning electron microscopy (SEM) image), while (C) is a high-resolution TEM image. Arrows in (B) indicate ellipsoidal particles lying on their sides.

electron microscopy (TEM), as shown in Figure 1B. These particles have average lengths and widths of ~130 nm and ~45 nm, respectively. The high-magnification TEM image in Figure 1C reveals the unusual texture of the particles, which are built up of numerous small nanoparticles roughly 6–7 nm in size. It appears that these primary small nanoparticles interconnected with one another to form larger secondary ellipsoidal architectures with recognizable boundaries or voids between the component subunits. An average particle size in good agreement with the TEM observation was determined from the X-ray diffraction data using the Debye–Scherrer formula. The XRD line broadening results from the small grain sizes of the ellipsoidal aggregates, the lattice imperfections, and stacking faults in the contacting/connecting areas between neighboring particles. This provides further insight into the mechanism of aggregation growth of small cupric oxide nanoparticles.

The high-resolution (HR) TEM image of a single ellipsoidal nanostructure in Figure 2A clearly shows the obvious aggregation of small nanoparticles. The selected area electron diffraction (SAED) pattern of the same single nanoarchitecture in Figure 2B can also be indexed to the monoclinic structure of cupric oxide with phase purity. It is surprising that the nanostructure built up from particles exhibits an almost single-crystalline diffraction pattern with its spot-like appearance along the [001] axis of crystalline cupric oxide. The slightly elongated diffraction spots suggest the presence of multiple nanodomains with a small misorientation deviating from perfect alignment between nanocrystallites in the resulting ellipsoidal nanoarchitecture. The average orientation distribution was estimated to be ~5°, measured from the arc angles/lengths in the diffraction pattern. The elongated diffraction spots in SAED may result from lattice orientation imperfections among the primary particles prepared at room temperature. This was referred to as imperfect-orientation attachment

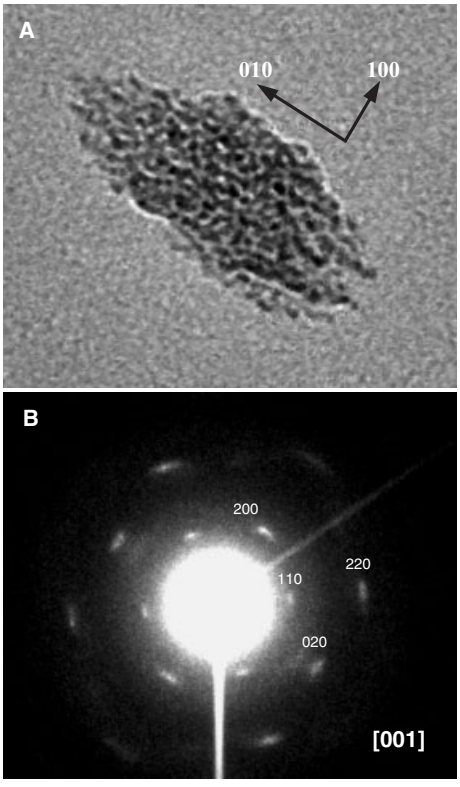

Figure 2. A) High-resolution TEM image and B) selected area electron diffraction (SAED) pattern of a single CuO ellipsoidal particle.

ADVANCED MATERIALS

in hydrothermally treated anatase and bio-generated iron oxyhydroxide by Banfield and co-workers.[6,9]

It was also observed that all the SAED patterns of single isolated ellipsoids show identical diffraction patterns along the [001] direction of cupric oxide. This is attributed to the flat nature of the ellipsoidal particles, which tend to lie flat on the TEM copper grid as shown in Figure 1B. In fact, several rod-like particles were also observed in the overview TEM image in Figure 1B. This is because ellipsoidal particles lying on their side by chance can display a rod-like shape with very thin tips (as indicated by arrows). The as-synthesized nanostructures may thus have smaller thicknesses of roughly 10–15 nm (lateral dimension), but larger lengths and widths of ~130 nm and ~45 nm, respectively.

The aggregation-based growth of a few hundred nanoparticles into single-crystalline assemblies of CuO nanoparticles is schematically illustrated in Figure 3. The size scales of the as-synthesized ellipsoids are very different in all three dimensions (in the *a*-, *b*-, and *c*-axes). It depends on the number of

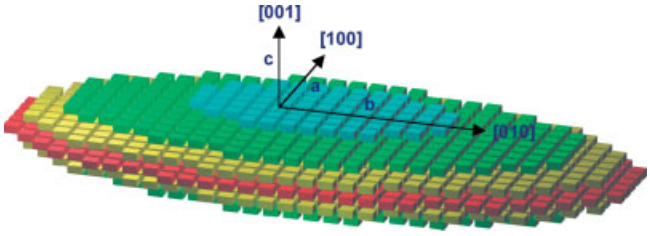

Figure 3. Schematic illustration of a single-crystalline assembly of cupric oxide built from aggregated nanoparticles.

particles aggregated in the direction of the particular axis. From the TEM images shown in Figure 1C and Figure 2A, anisotropic growth rates of the ellipsoidal particles are ordered as follows: $b > a > c$ (or [010] > [100] > [001]), indicating different particle-aggregation potentials. Aggregation and attachment occurs preferentially between the (010) lattice planes of nanoparticles. The preferential anisotropic growth is different from the classical crystal growth of cupric oxide nanowires along the [111] direction reported in the literature.[20,22]

To obtain a better understanding of the anisotropic growth mechanism of ellipsoidal particles, we collected reaction products at different growth stages for TEM and SAED investigation (Fig. 4). At an early reaction stage (after 2 h), small CuO nanocrystals about 6–7 nm in diameter were formed, as shown in Figure 4A. The particle size is consistent with the subunit size in the final ellipsoidal architectures. This provides direct evidence that the architecture did result from particle-by-particle aggregation growth rather than classical atom-by-atom addition. The SAED in Figure 4A, taken from the dense region of primary particles, shows typical diffraction rings from polycrystalline CuO. The (110), (200), and (020) rings can be assigned to the diffraction pattern of CuO along the [001] zone axis, which is further confirmed by our simulated electron diffraction patterns of mono- and polycrystalline CuO. The specific diffraction pattern suggests that these small nanoparticles have preferentially oriented their [001] crystallographic directions parallel to the *c*-axis. However, their [100] and [010] directions are still random, which leads to polycrystalline diffraction rings along the [001] axis. The HRTEM image in Figure 4B reveals the crystalline nature of a few CuO nanoparticles with straight (200) lattice fringes. The orientation of the CuO particles at an early stage was also disclosed by the observation of identical (200) lattice planes, but with various lattice directions, in these primary particles, indicating that the preferential orientation of their [001] crystal directions is parallel to the *c*-axis.

When the aging time was extended to 5 h, CuO nanoparticles in the mother solution can be removed by centrifugation to leave a colorless supernatant solution, indicating the complete depletion of copper-complex precursors or complete formation of CuO nanoparticles. Meanwhile, some primary particles began to stick together loosely. After 24 h, these small aggregates had grown into larger ellipsoidal nanostructures with observable boundaries or voids between particles through stacking of more particles (Fig. 4C). All primary nanoparticles in the reaction solution were completely organized into larger aggregates because none of them were observed in the mother solution by TEM. The SAED pattern of the single aggregate (Fig. 4C) shows bright diffraction arcs accompanied by faint [001] polycrystalline rings. Those bright arcs correspond to the diffraction spots of the crystalline CuO architecture, which clearly reveals that small particles in aggregates have roughly oriented their [100] and [010] crystallographic directions to common *a*- and *b*-axes, respectively. The orientation along the [100] and [010] crystallographic directions thus weakens the intensity of the diffraction rings, as shown in Figure 4C. During subsequent aging for a week, the secondary particles further undergo restructuring and rearrangement, resulting in more compact and regular ellipsoidal aggregates. A large number of CuO nanoparticles in the aggregates adopted identical crystallographic directions in all three dimensions. Figure 4D also shows the clear diffraction spots of a single monoclinic cupric oxide aggregate, which is the same as the one in Figure 2B. The above results demonstrate a three-step growth process to form final organized aggregates in our reaction system, as shown in Figure 5.

Aggregation is energetically favored because the formation of larger crystals can greatly reduce the interfacial energy of small primary nanoparticles. Strong organic ligands usually promote self-assembly of nanoparticles, driven by the interactions between organic ligands adsorbed on different particles. However, weakly protected nanoparticles often undergo entropy-driven random aggregation through strong interactions between the particles themselves due to the facile desorption and exchange of ligands. The moderate binding affinity of ligands such as formamide to copper ions[23–25] may provide the capability for controlled removal of the appropriate organic ligands at interfaces for subsequent oriented

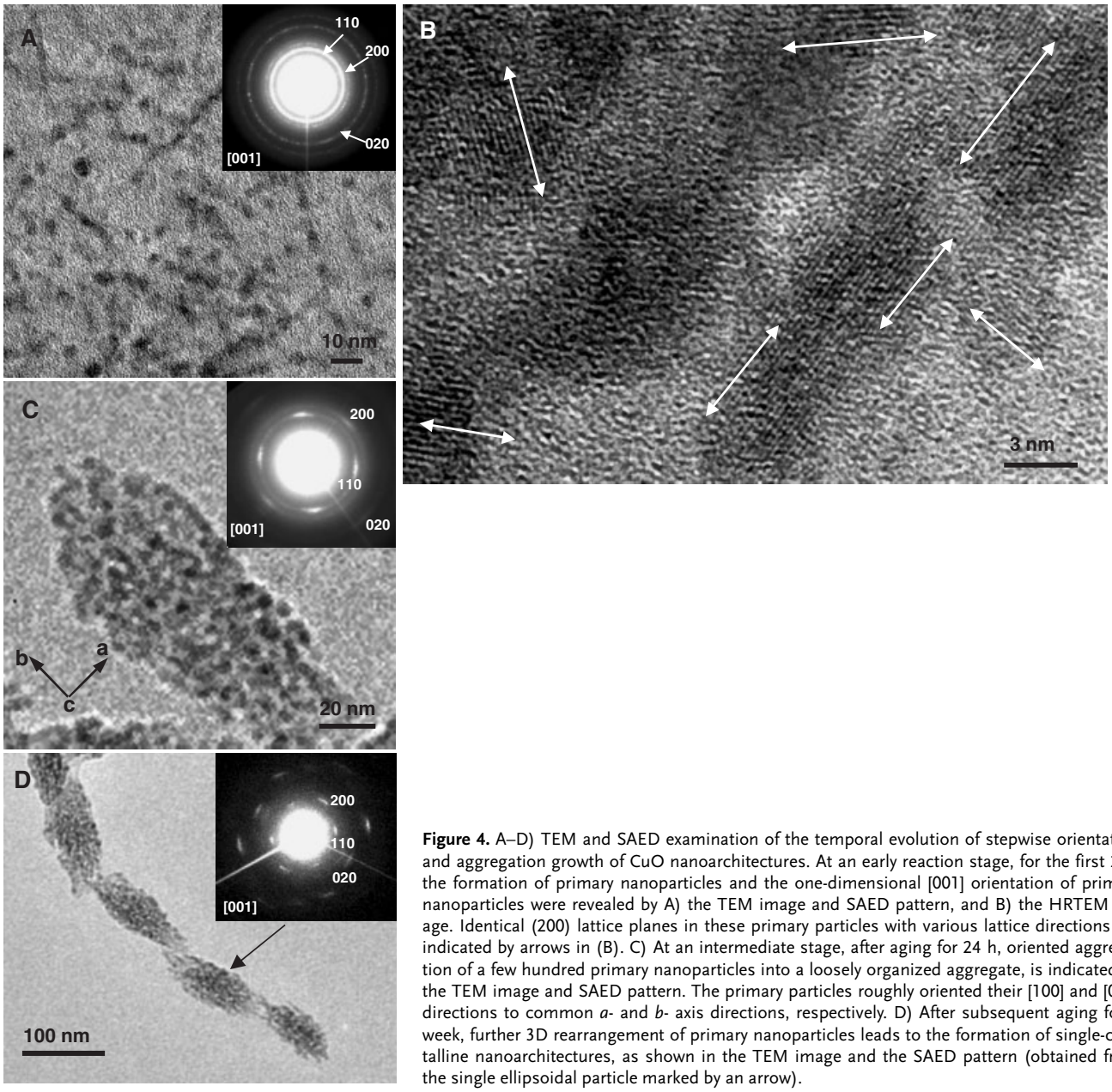

Figure 4. A–D) TEM and SAED examination of the temporal evolution of stepwise orientation and aggregation growth of CuO nanoarchitectures. At an early reaction stage, for the first 2 h, the formation of primary nanoparticles and the one-dimensional [001] orientation of primary nanoparticles were revealed by A) the TEM image and SAED pattern, and B) the HRTEM image. Identical (200) lattice planes in these primary particles with various lattice directions are indicated by arrows in (B). C) At an intermediate stage, after aging for 24 h, oriented aggregation of a few hundred primary nanoparticles into a loosely organized aggregate, is indicated by the TEM image and SAED pattern. The primary particles roughly oriented their [100] and [010] directions to common *a*- and *b*- axis directions, respectively. D) After subsequent aging for a week, further 3D rearrangement of primary nanoparticles leads to the formation of single-crystalline nanoarchitectures, as shown in the TEM image and the SAED pattern (obtained from the single ellipsoidal particle marked by an arrow).

attachment of nanoparticles to form ordered aggregates. Although the oxygen and nitrogen of formamide molecules are candidate donor atoms for coordination to copper ions, it was previously observed by IR and extended X-ray absorption fine structure (EXAFS) spectroscopy that the molecular structure of the formamide molecule prevents the nitrogen atoms from acting as coordinating atoms to form $Cu(HCONH_2)_4^{2+}$.[23,26] Selective adsorption of organic molecules to specific crystal surfaces has recently been extensively studied.[12,27,28] In the research reported here, the different amounts of formamide-molecule oxygen atoms adsorbed on different surface planes may depend on the corresponding surface density of copper atoms. Copper atom densities on (001), (010), and (100) planes of monoclinic CuO are calculated to be 12.5 atoms nm^{-2}, 8.5 atoms nm^{-2}, and 11.5 atoms nm^{-2}, respectively. The most stable surface plane should be (001), with the highest density of copper atoms and where formamide molecules are adsorbed more densely, resulting in a weak aggregation driving force along the *c*-axis. In contrast, the least-stable surface plane should be (010), with the lowest density of copper atoms and where formamide molecules are adsorbed more sparsely, resulting in preferential aggregation growth along the *b*-axis. The difference in the amount of formamide molecules adsorbed on various crystallographic planes may lead to the anisotropic aggregation-based growth of primary particles. The self-organized aggre-

ADVANCED MATERIALS

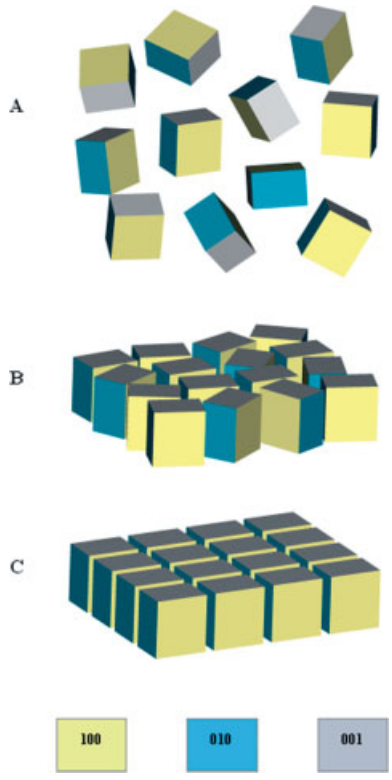

Figure 5. Schematic illustration of stepwise orientation and aggregation of a large number of primary nanoparticles into a monocrystalline structure.

gates gradually transform themselves into uniform ellipsoidal architectures, which are built up of much smaller primary particles as shown in Figure 1C. As in our case Ostwald ripening is not an obvious process at room temperature, only the aggregation process is involved in forming the final nanoparticle-built product. This is why we can observe the clear stepwise orientation and aggregation of a few hundred nanoparticles into defective single-crystalline architectures in three dimensions.

In summary, we have demonstrated the aggregation-based formation of uniform nanoparticle-built monocrystals by 3D-oriented aggregation of a few hundred CuO nanoparticles through rotation of adjacent nanoparticles so that they share identical crystallographic planes. Stepwise orientation and aggregation in three dimensions has been observed at room temperature, resulting from the formation of primary CuO nanoparticles in mother solution via the preferential 1D [001] orientation of a limited number of nanoparticles at an early stage, to the eventual 3D-oriented aggregation of a few hundred nanoparticles into a monocrystalline structure. Selective adsorption of formamide molecules on various crystallographic planes may play an important role in the anisotropic growth of ellipsoidal nanoarchitectures. An understanding of the 3D-oriented attachment will be helpful in controlling the aggregation-driven formation of ordered nanostructured materials and will provide new insights into mineralization mechanisms.

Experimental

Typically, a piece of pure copper foil (10 mm × 10 mm × 0.127 mm) was immersed into formamide (2 mL) in a 10 mL vial at room temperature. Copper metal was oxidized slowly by naturally dissolved oxygen in formamide (< 0.05 % water). Cu^{2+} ions were continuously released from copper foil into formamide (without introducing counterions of copper ions, such as $CuCl_2$ salt, that is used in other synthetic approaches), while oxygen was simultaneously reduced: [29–31]

$$O_2 + 2\,H_2O + 4\,e^- \rightarrow 4\,OH^- \quad (1)$$

With increasing reaction time, the solution gradually changed from colorless to light blue, and eventually to deep blue. This indicates the formation of $[Cu(HCONH_2)_4]^{2+}$-complex ions (the structure was previously reported in the literature [23]), because copper ions can be immediately captured and coordinated by formamide molecules, forming copper-complex ions after release from copper metal:

$$Cu + 1/2\,O_2 + H_2O + 4\,HCONH_2 \rightarrow [Cu(HCONH_2)_4]^{2+} + 2\,OH^- \quad (2)$$

After six days, a total concentration of copper-complex ions of up to 60 mM was reached, as measured by atomic emission spectroscopy. The resulting solution was then diluted by a factor of five with deionized water (0.2 mL original solution was mixed with 1 mL water). The mixture solution was left to stand at room temperature and a brownish-black precipitate was apparent after ~12 h. The flocculent precipitate was further aged for one week before samples were isolated for measurement.

The X-ray diffraction pattern of CuO particles was recorded using a Bruker AXS GADDS X-ray diffractometer. The crystalline structure of the CuO particles was analyzed by means of a JEOL 3010 transmission electron microscope. The morphology of the CuO particles was examined using a JEOL JSM-6700 field-emission scanning electron microscope. Copper-ion concentrations were measured by inductively coupled plasma–atomic emission spectrometry using a Perkin–Elmer Optima 3000 spectrometer.

Received: March 17, 2004
Final version: August 1, 2004

[1] G. M. Whitesides, B. Grzybowski, *Science* **2002**, *295*, 2418.
[2] Z. L. Wang, *Adv. Mater.* **1998**, *10*, 13.
[3] H. Weller, *Philos. Trans. R. Soc. London, Ser. A* **2003**, *361*, 229.
[4] K. J. C. van Bommel, A. Friggeri, S. Shinkai, *Angew. Chem. Int. Ed.* **2003**, *42*, 980.
[5] M. Li, H. Schnablegger, S. Mann, *Nature* **1999**, *402*, 393.
[6] J. F. Banfield, S. A. Welch, H. Z. Zhang, T. T. Ebert, R. L. Penn, *Science* **2000**, *289*, 751.
[7] C. Pacholski, A. Kornowski, H. Weller, *Angew. Chem. Int. Ed.* **2002**, *41*, 1188.
[8] Z. Tang, N. A. Kotov, M. Giersig, *Science* **2002**, *297*, 237.
[9] R. L. Penn, J. F. Banfield, *Science* **1998**, *281*, 969.
[10] Z. P. Zhang, M. Y. Han, *Chem. Phys. Lett.* **2003**, *374*, 91.
[11] B. A. Korgel, D. Fitzmaurice, *Adv. Mater.* **1998**, *10*, 661.
[12] R. C. Jin, Y. C. Cao, E. C. Hao, G. S. Metraux, G. C. Schatz, C. A. Mirkin, *Nature* **2003**, *425*, 487.
[13] J. Polleux, N. Pinna, M. Antonietti, M. Niederberger, *Adv. Mater.* **2004**, *16*, 436.
[14] M. Niederberger, F. Krumeich, K. Hegetschweiler, R. Nesper, *Chem. Mater.* **2002**, *14*, 78.
[15] T. Sugimoto, A. Muramatsu, *J. Colloid Interface Sci.* **1996**, *184*, 626.
[16] C. L. Carnes, J. Stipp, K. J. Klabunde, *Langmuir* **2002**, *18*, 1352.
[17] K. Borgohain, J. B. Singh, M. V. Rama, S. Mahamuni, *Phys. Rev. B: Condens. Matter Mater. Phys.* **2000**, *61*, 11 093.
[18] C. Xu, Y. Liu, G. Xu, G. Wang, *Mater. Res. Bull.* **2002**, *37*, 2365.
[19] Z. S. Hong, Y. Cao, J. F. Deng, *Mater. Lett.* **2002**, *52*, 34.
[20] X. C. Jiang, T. Herricks, Y. N. Xia, *Nano Lett.* **2002**, *2*, 1333.

[21] L. F. Gou, C. J. Murphy, *Nano Lett.* **2003**, *3*, 231.
[22] W. Wang, Z. Liu, Y. Liu, C. Xu, C. Zheng, G. Wang, *Appl. Phys. A: Mater. Sci. Process.* **2003**, *76*, 417.
[23] M. Sano, T. Maruo, H. Yamatera, *J. Chem. Phys.* **1988**, *89*, 1185.
[24] W. Zamudio, A. M. Garcia, R. Baraona, *Transition Met. Chem. (Dordrecht, Neth.)* **1995**, *20*, 518.
[25] A. Luna, B. Amekraz, J. Tortajada, J. P. Morizur, M. Alcami, O. Mo, M. Yanez, *J. Am. Chem. Soc.* **1998**, *120*, 5411.
[26] M. S. Barvinok, L. V. Mashkov, L. A. Obozova, *Zh. Neorg. Khim.* **1975**, *20*, 429.
[27] X. G. Peng, *Adv. Mater.* **2003**, *15*, 459.
[28] S. M. Lee, S. N. Cho, J. Cheon, *Adv. Mater.* **2003**, *15*, 441.
[29] L. Sobolewski, *J. Photochem. Photobiol., A* **1995**, *89*, 89.
[30] N. Mora, E. Cano, E. M. Mora, J. M. Bastidas, *Biomaterials* **2002**, *23*, 667.
[31] A. López-Delgado, E. Cano, J. M. Bastidas, F. A. López, *J. Mater. Sci.* **2001**, *36*, 5203.

Large-Scale Design of Cubic *Ia3d* Mesoporous Silica Monoliths with High Order, Controlled Pores, and Hydrothermal Stability**

By *Sherif A. El-Safty*,* *Takaaki Hanaoka*, and *Fujio Mizukami**

Periodically mesoporous materials with two- and three-dimensional (2D and 3D) structures are one of the most exciting new developments in materials science and technology in the last decade. Features of these mesoscale architectures include controllable mesopore size (20–300 Å) which enable these materials to be promising candidates in applications such as catalysis, separations, sensing, and optical and electronic systems.[1] Since the discovery of the prominent class of the M41S mesoporous family, surfactant-templated synthesis approaches are commonly used to direct the design of materials.[2] The nature of these amphiphiles enable successful fabrication of highly ordered nanoscale structures.[2,3] The resultant 3D cubic mesoporous materials will find many industrial applications.[1] Among these 3D structures, a cubic *Ia3d* symmetry (MCM-48) with a periodic gyroid surface and bicontinuous networks could show particular promise for advanced functionalities. Initially, MCM-48 materials were fabricated using cationic alkylammonium surfactants,[2] cationic/D-maltoside mixtures,[4] and mixed cationic/nonionic or anionic surfactants.[5] However, the more restrictive syntheses (under basic conditions) and the limited pore sizes up to 4.0 nm have inhibited the utility of these MCM-48 materials, particularly in inclusion chemistry.[1]

Recently, powdery cubic *Ia3d* mesoporous silica with large pores (> 5 nm in diameter) was fabricated using diluted block copolymer solutions under acidic conditions,[6] and a high-quality cubic structure with *Ia3d* symmetry was successfully fabricated using diblock poly(ethylene oxide)-poly(methyl acrylate) copolymers (laboratory synthesis polymers)[6a] and triblock copolymer P123 ($EO_{20}PO_{70}EO_{20}$, EO = ethylene oxide, PO = propylene oxide)-assisted additive synthesis routes, such as sulfur-containing silane (3-mercaptopropyltrimethoxysilane),[6b] NaI salt,[6c] and butanol.[6d] These large mesoscopically organized cubic *Ia3d* materials can be used in widespread applications, as for MCM-48 mesostructured materials.[5] However, even in these syntheses of gyroidal cubic *Ia3d* materials,[6] the intensive and time-consuming synthesis conditions, and the powdery nature of the products, could constrain their practical utility. If the mesostructured composites are fabricated into monoliths that are hard, translucent, and crack-free, with macroscopic length scale and with a 3D cubic ordered framework in large domain sizes, their applications can be widely expanded.[7]

The major challenge in the design of such periodic mesoporous composites (monolith, and powder forms) is in improving their thermal/hydrothermal stabilities; because of the amorphous atomic scale of the network pores, however, the periodic order structures might collapse under hydrothermal treatments such as boiling or steaming. This tendency for structural collapse under such hydrothermal treatment has diminished their functionality, particularly in industrial applications. A significant effort to improve these mesoporous structural properties has led to increased hydrothermal stability of the resultant materials.[8] Another major challenge in the fabrication process is reliable control over the actual microstructure phase of the templates and the final composite replica.[9,10] Hence, the direct synthesis of surfactant–silica mesophases is expected to open the possibility of designing highly crystalline mesoporous materials with a variety of mesoscopic structures.[9a,b,10] Important developments in the direct-templating methodology were provided by using *instantly preformed liquid-crystalline phases* of surfactant in bulk lyotropic and microemulsion systems, as we recently reported.[11] This development strategy shows promise for high fidelity of control over the phase morphology. However, various dimensional structures (lamellar, 2D hexagonal, and 3D cubic lattices) were easily fabricated by using inexpensive commercial nonionic surfactants (Brij-types) as organizing agents under acidic conditions, yet long-range order frameworks were attained with most of the geometrical structures.[11]

Here, periodically gyroidal cubic *Ia3d* monolithic silica (HOM-5) with large cylindrical opened pores (up to 10 nm in diameter) was fabricated for the first time using the instant direct-templating method in bulk lyotropic and microemulsion systems of P123 copolymers. Transmission electron microscopy (TEM) images of HOM-5 show that wagon-wheel-like

[*] Dr. S. A. El-Safty, Dr. F. Mizukami, Dr. T. Hanaoka
Laboratory for Membrane Chemistry, Tohoku Center
National Institute of Advanced Industrial Science
and Technology (AIST)
4-2-1 Nigatake, Miyagino-ku, Sendai, 983-8551 (Japan)
E-mail: sherif.el-safty@aist.go.jp; f.mizukami@aist.go.jp

[**] Supporting Information is available online at Wiley Interscience or from the author.

 DOI: 10.1002/adma.200401317